Journal of Luminescence 204 (2018) 513–519

Contents lists available at ScienceDirect

Journal of Luminescence

journal homepage: www.elsevier.com/locate/jlumin

Structural and spectroscopic properties of Eu^{3+} doped $Y_4Al_2O_9$ compounds through a soft chemical process

G. Gasparotto[a], L.S. Tavares[a], T.C. Silva[b], L.J.Q. Maia[a,*], J.F. Carvalho[a]

[a] Instituto de Física, UFG, Campus Samambaia, Av.Esperança s/n, CEP 74690-900 Goiânia, GO, Brazil
[b] Departamento de Química Geral e Inorgânica, Instituto de Química, UNESP, C.P. 355, CEP 14801-970 Araraquara, SP, Brazil

ARTICLE INFO

Keywords:
YAM
Europium
Occupation sites
Judd-Ofelt intensity parameters
Visible emissions

ABSTRACT

The present work reports on the synthesis, structural and optical properties of $(Y_{1-x}Eu_x)_4Al_2O_9$ powders, with x ranging from 0.001 to 0.030. We prepared the materials using a modified polymeric precursors method, and the effect of annealing temperature and Eu^{3+} concentrations were evaluated. Structural and microstructural parameters, such as cell parameters, crystallite size and grain size were determined and evaluated by using the results from X-ray diffraction and high-resolution transmission electron microscopy techniques. An annealing temperature of 800 °C was enough to obtain single $Y_4Al_2O_9$ crystalline phase with good distribution of Eu^{3+} ions. Diffuse reflectance spectra and optical bandgap of 4.52 eV for $(Y_{0.995}Eu_{0.005})_4Al_2O_9$ – determined by Kubelka-Munk model – showed good optical quality of the samples, which were considered non-conducting. All doped samples possessed visible photoluminescence emission from Eu^{3+} ions under excitation at 393 nm, with higher emissions occurring in the red region from $^5D_0 \rightarrow {}^7F_2$ transition, with R/O relation of 1.69 for the sample with x = 0.010. Analyzing photoluminescence emission spectra, the lifetime values and Judd-Ofelt parameters, we determined that Eu^{3+} occupied three different sites of the $Y_4Al_2O_9$ (YAM) structure, replacing Y^{3+} ions, with the quenching concentration occurring between x = 0.020 and x = 0.030. We noted that Eu^{3+} ions are in a chemical environment with low polarization, and their degree of covalence is low. Finally, samples with x = 0.020 $(Y_{0.980}Eu_{0.020})_4Al_2O_9$ seems to be useful as red phosphors.

1. Introduction

The Al_2O_3-Y_2O_3 system has been studied for its great importance to several optical devices, especially lasers. This system presents four crystalline phases: $YAlO_3$ (YAP) with orthorhombic perovskite structure, $YAlO_3$ (YAH) with hexagonal structure, $Y_3Al_5O_{12}$ (YAG) with cubic garnet structure and $Y_4Al_2O_9$ (YAM) with monoclinic structure [1,2]. YAG and YAP have been extensively studied, but only a few works are likely related to the YAM phase structure, having $P2_1/c$ space group, aluminium atoms coordinated to four oxygen atoms and yttrium atoms coordinated to six or seven oxygen atoms, being YO_6 and YO_7 polyhedra, respectively, and Y^{3+} have C_1 point symmetries.

The YAM phase can be found as monocrystals [3] and polycrystals [4–8]. Polycrystals can be obtained from a solid-state reaction [4] and from chemical synthesis [5–8]. The solid-state reaction requires a relatively high temperature (near the components' melting point); that said, the chemical synthesis has attracted interest because it requires lower temperature than does the solid-state reaction. Some studies report synthesis by a molten salt process followed by a chemical co-precipitation [5], solvothermal reaction [6], polymeric precursor method (Pechini method) [7] and sol-gel process [8]. When compared with the other methods, the main advantage of the polymeric precursor method (considered a soft chemical process) is its homogeneous distribution of chemical elements in the solution, which can be maintained until the end of the procedure to obtain powders and thin films. The polymeric precursor method is attractive because it does not require a special atmosphere, but its main disadvantage is related to high amounts of organic materials (such as citric acid and polyalcohol) for ion complexation and polymerization. However, heat treatments higher than 700 °C will efficiently remove the organic constituents.

Eu^{3+} doped YAM [3–19] were prepared, and some photoluminescent studies were performed for visible emitting devices and structural probes. Ma et al. [5] studied the $(Y_{1-x}Eu_x)_4Al_2O_9$ composition with x ranging from 0 to 0.60 and found that x = 0.10 presented a maximum photoluminescence (PL) emission; in higher concentrations, the quenching effects took place. But in the study developed by Yadav et al. [16] from x = 0.01 to x = 0.50, the highest PL emission occurred for x = 0.20. Nonetheless, Upadhyay et al. [4] studying Eu^{3+} doped

* Corresponding author.
E-mail address: lauro@ufg.br (L.J.Q. Maia).

https://doi.org/10.1016/j.jlumin.2018.08.055
Received 3 April 2018; Received in revised form 16 August 2018; Accepted 17 August 2018
Available online 21 August 2018

YAM with x between 0.003 and 0.0375 (0.2 and 2.5 mol%) described that the best composition was that with x = 0.03 (2 mol%). Finally, Dubey et al. [18], analyzing compositions with x ranging from 0.0015 to 0.0375 (0.1 a 2.5 mol%), mentioned that the best was that with x = 0.0225 (1.5 mol%). As we can see, the best doping level is controversial and, certainly, depends on the synthesis method and distribution of Eu^{3+} ions into the host.

The great interest on the optical properties of YAM is related to its multisite structure. Normally, Eu^{3+} ions can be used as structural probes and as red/orange emitters for displays [7,16,20]. The study of occupation sites is vital to understanding the photoluminescent features and the ion–ion interaction mechanisms that lead to photoluminescence quenching. Thereby, the synthesis with other lanthanide ions can be planned for used as nanothermometers, solar energy concentrators and laser devices [21–26].

A previous study of Eu^{3+} doped YAM phase developed by Kaczkan et al. [3] claimed that the band number of $^5D_0 \rightarrow {}^7F_0$ transition reflects the number of sites occupied by Eu^{3+} ions. Also, Jung et al. [6], Liu et al. [8] and Yadav et al. [9] observed that Eu^{3+} ions occupy two different sites of YAM structure, while Kaczkan et al. [3] reported occupation of three different sites. The literature has no consensus regarding the number of Y^{3+} sites in YAM that can be replaced by Eu^{3+}. In fact, the maximum cited has been four sites, but the number of occupied sites can be associated to the Eu^{3+} amounts. Further studies are required.

In this paper, the $(Y_{1-x}Eu_x)_4Al_2O_9$ compositions, with x ranging from 0.001 to 0.030, were prepared using a modified polymeric precursor method and annealed from 800 °C to 1100 °C. Structural and microstructural properties were evaluated by X-ray diffraction patterns, Rietveld refinements, high-resolution transmission electron microscopy, and selected area electron diffraction techniques. Diffuse reflectance spectra, PL emission spectra and the lifetime of Eu^{3+} $^5D_0$ level were determined and evaluated. Finally, Judd-Ofelt (J-O) intensity parameters were calculated and different sites occupied by Eu^{3+} ions in the YAM host structure were investigated.

2. Experimental method

The crystalline powders of $(Y_{1-x}Eu_x)_4Al_2O_9$ composition with x = 0.001, 0.005, 0.010, 0.020 and 0.030 were synthesized by the modified polymeric precursors method [27]. The synthesis used yttrium nitrate hexahydrate ($Y(NO_3)_3{\cdot}6H_2O$) (Sigma-Aldrich, 99.8%), aluminium nitrate nonahydrate ($Al(NO_3)_3{\cdot}9H_2O$) (Sigma-Aldrich, 99.8%), and europium nitrate pentahydrate ($Eu(NO_3)_3{\cdot}5H_2O$) (Sigma-Aldrich, 99.9%) as metal precursors. First, at room temperature, the reactants were dissolved in distilled water under vigorous magnetic stirring, followed by the addition of citric acid ($C_6H_8O_7$, Sigma-Aldrich ≥ 98%), the molar ratio of citric acid to metal was 3:1. D-Sorbitol (Sigma-Aldrich, 98%) was added to the metal-citrate solution, with a citric acid molar ratio of 3:2 to promote the metallic citrates polymerization. The formed resin was dried at 250 °C, resulting in a black solid that was deagglomerated in an agate mortar and annealed at 700 °C for 12 h under N_2 flux. Then the powders were separated into portions and heat-treated (HT) between 800 °C and 1100 °C for 3 h.

The crystalline phases were identified by an X-ray diffraction (XRD) technique using a Bruker D8 Discover diffractometer operating at 40 kV and 40 mA, with monochromatic radiation from a copper anode tube coupled to a Johansson monochromator for $K\alpha_1$ (λ = 1.54059 Å). The configuration used was the Bragg-Brentano θ–2θ geometry, with a range of 2θ from 5° to 100° and step of 0.01°. The structure refinement was performed using the Rietveld method with TOPAS software version 4.2.

The microstructure of the samples was analyzed with a high-resolution transmission electron microscope (HRTEM) incorporating JEOL JEM-2100 equipment operating at 200 kV and an electron diffraction (SAED) pattern from the selected area. The samples were diluted in isopropyl alcohol and deposited on metallic grids covered with a carbon thin film.

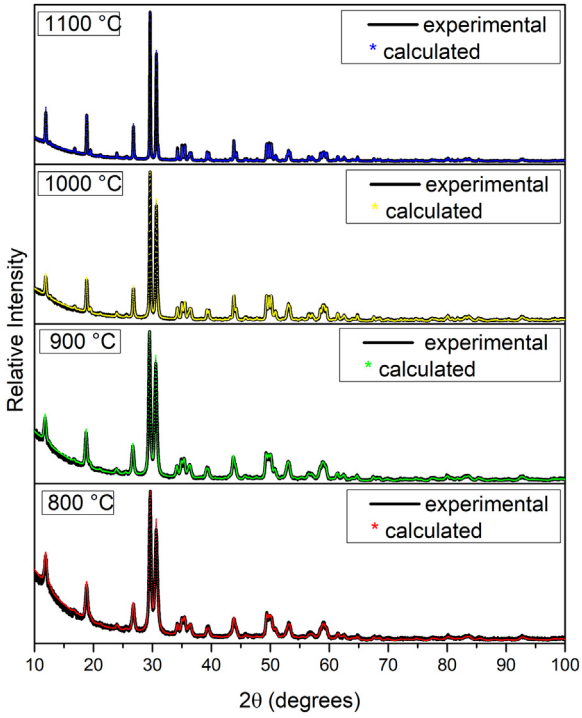

Fig. 1. X-ray diffractograms (solid lines, ——) and Rietveld refinement (symbols, *) for the $(Y_{0.995}Eu_{0.005})_4Al_2O_9$ powders heat-treated at 800 °C, 900 °C, 1000 °C, and 1100 °C.

Diffuse reflectance measurements were obtained using a PerkinElmer UV–Vis–NIR LAMBDA 1050WB spectrophotometer and a Praying Mantis® accessory. The standard reflectance material ($BaSO_4$ powder) was purchased from Sigma-Aldrich and used as received.

PL emission spectra were performed at room temperature using a HORIBA Jobin Yvon Fluorolog FL-3-221 spectrofluorometer, equipped with double monochromator and a Hamamatsu photomultiplier tube. For excitation, we employed a continuous 450 W Xe arc lamp. PL emission spectra were corrected for the spectral response of the monochromators and the detector using a typical correction spectrum provided by the manufacturer. The PL decay curves at 612 nm were obtained under excitation at 394 nm using a pulsed Xe lamp (3 μs bandwidth) in a HORIBA Jobin Yvon Fluorolog FL-3-222 spectrofluorometer.

3. Results and discussion

Fig. 1 shows the experimental X-ray diffraction patterns of $(Y_{0.995}Eu_{0.005})_4Al_2O_9$ (x = 0.005) powders HT at 800 °C, 900 °C, 1000 °C and 1100 °C (solid lines), and the Rietveld refinements for all samples (symbols). It was observed that annealing at 800 °C was enough to obtain pure YAM phase, proving the efficiency of the chemical process employed. At higher temperatures, similar X-ray diffraction patterns were collected, with a gradual reduction of full-width at half maximum (FWHM) diffraction peaks (effect of narrowing) and intensity increasing due to increase of crystallinity and likely to crystallite growth.

We verified the monoclinic structure of YAM phase (space group $P2_1/c$), with cell parameters: a = 7.376(7) Å, b = 10.460(1) Å, c = 11.120(1) Å, and β = 108.610(5)° for HT at 800 °C, similar to those from the literature (a = 7.378 Å, b = 10.474 Å, c = 11.125 Å, and β = 108.540°) [3,28].

The YAM structure contains four yttrium sites (two YO_6 and two YO_7). Y^{3+} ions have C_1 point symmetry and these sites can be occupied

by lanthanide ions, especially Eu^{3+} due to its ionic radius similarity to Y^{3+} (1.13 Å for Eu^{3+} and 1.06 Å for Y^{3+}) [29], a larger radius compared to Al^{3+} (0.53 Å) [30]. By using the X-ray diffraction technique, the formation of a single YAM phase indicates a good Y^{3+} ions replacement by Eu^{3+} ions.

In the literature, there is only one work – developed by Wang et al. [7] – on the synthesis by the polymeric precursors method of Eu^{3+} doped YAM. However, the synthesis temperature employed by Wang and colleagues was 1000 °C, higher than that observed in our work. We reduced 200 °C of temperature synthesis, which can be related to the use of D-sorbitol as a polymerizing agent and intermediate HT at 700 °C during 12 h under N_2 flux. Meanwhile, HT at 1100 °C appears to be the best for obtaining the highest YAM crystallinity; this was used as the synthesis temperature for Eu^{3+} concentration variation to evaluate the spectroscopic behavior.

Rietveld refinement is a method by which the intensity profile is measured and allows for an approximate model with a true structure. Refinement was performed starting from the structural data ICSD-63650 file [31]. We observed good agreement between the experimental and calculated XRD patterns, indicating a successful refinement method.

Table 1 lists the values obtained through Rietveld refinement as well as the structural parameters, cell volume, G_{of} and R_{wp} coefficients. In comparing the results of the refinement with the results of the ICSD-63650 file [31], we did not observe a significant difference in the values of all parameters; that is, the HT temperature did not affect significantly any parameter. The reliability parameter (G_{of}) value was close to unity, demonstrating a good agreement between experimental and calculated data.

Table 1 also shows the crystallite size values as a function of HT temperature. The crystallite size was calculated from the FWHM of the X-ray diffraction peaks using Scherrer's equation [32,33]. The (122) crystallographic peak of YAM phase was used to determine the crystallite size, and the Scherrer's equation is:

$$D_{hkl} = \lambda\, k/\beta \cos\theta, \quad (1)$$

where λ is the wavelength (Cu $K\alpha_1$), θ is the diffraction angle, k is a constant and β is the corrected half-width of the diffraction peak. The diffraction peak profile was fitted using a pseudo-Voigt function to calculate the FHWM. The β-value was calculated considering the following relation:

$$\beta = (B_{obs}^2 - B_s^2)^{1/2} \quad (2)$$

where B_{obs} is the FWHM of the sample and B_s is that of the external standard (corundum).

As we see in Table 1, increasing the HT temperature from 800 °C to 1100 °C, the crystallite size increased from 34 nm to 120 nm, respectively, due to crystallinity improvements. The higher mobility of Al^{3+} and Y^{3+} ions [2] leads to crystallite growths. As mentioned by Carvalho et al. [2], the significant differences in chemical bonding and mobilities of Al^{3+} and Y^{3+} ions favor the formation of YAM phase at a lower temperature (885 °C) than YAH (hexagonal $YAlO_3$, at 909 °C), YAG (at 1010 °C) and YAP (at 1075 °C) phases.

Fig. 2a and b shows TEM and HRTEM images of $(Y_{0.995}Eu_{0.005})_4Al_2O_9$ sample HT at 1100 °C, respectively. We can see in Fig. 2a that grains ~ 80 nm in diameter formed a large agglomerate due to a coalescence effect. These particles have high crystallinity. A well-defined atomic plane of 3.87 Å was observed and attributed to the (002) plane of the monoclinic YAM phase. The SAED patterns in Fig. 2c reveal that the particles were monocrystals, in agreement with planes in JCPDS card No. 83–0935 and confirming the crystallization of the $(Y_{0.995}Eu_{0.005})_4Al_2O_9$ phase.

Comparing the results presented above (Table 1) on crystallite size ranging from 34 to 86 nm with those from the work developed by Xia et al. [15], which vary from 28 to 34 nm using sol-gel process between 800 °C and 1000 °C, however Xi-ming et al. [12] obtained from 20 to 50 nm diameter particles. Despite, our polymeric precursor methodology produced higher crystallite sizes, but not so much higher than those from sol-gel process, and we demonstrated the possibility to produce nanometric particles of 86 nm at high temperatures (1000 °C). When cell parameters were compared, the values listed in Table 1 were similar to those from references [12,15].

Fig. 3a presents the diffuse reflectance spectrum in the UV–Vis–NIR region, 250–850 nm range, of the $(Y_{0.995}Eu_{0.005})_4Al_2O_9$ composition HT at 1100 °C. We observed that the spectrum has a large absorption band in the range from 350 nm to 400 nm due to some defects of the YAM monoclinic phase structure, which influence the optical bandgap value. These defects can be related to non-binding oxygens on the surface of crystallites and oxygen vacancies in the crystalline structure. Between 250 nm and 350 nm, there is an absorption band due to change transfer between metal-oxygen of the compound. A high reflectivity (higher than 90%) can be seen from 400 nm to 850 nm, attesting the optical quality of the $(Y_{0.995}Eu_{0.005})_4Al_2O_9$ crystalline powder.

The diffuse reflectance spectrum was used to determine the band gap value of the $(Y_{0.995}Eu_{0.005})_4Al_2O_9$ sample. It was also the procedure used and previously described by Maia et al. [34].

The remission function $F(R\infty)$ in the Kubelka-Munk model [35] is defined as:

$$F(R_\infty) = (1 - R_\infty)^2/2R_\infty \quad (3)$$

where R_∞ is the measured reflectance normalized by the standard $BaSO_4$ powder. The band gap (E_g) and the absorption coefficient (α) are correlated by the relation $\alpha h\nu = A(h\nu - E_g)^{1/2}$ in which $h\nu$ is the phonon energy and A is a proportionality constant. Then, the remission equation can be written as:

$$(F(R_\infty)h\nu)^2 = C(h\nu - E_g) \quad (4)$$

Thus, E_g is obtained from the linear fitting of $(F(R_\infty)h\nu)^2$ versus $h\nu$, and extrapolating to $(F(R_\infty)h\nu)^2 = 0$ in which $h\nu$ is equal to E_g, or E_g is the intercept of the fitting (green line) with the horizontal line, shown in Fig. 3b.

The bandgap value of our $(Y_{0.995}Eu_{0.005})_4Al_2O_9$ sample was of 4.52 eV, in good agreement with the literature values [36,37], with the sample considered non-conducting.

Fig. 4a shows the excitation PL spectra from $(Y_{1-x}Eu_x)_4Al_2O_9$ powders with x = 0.001, 0.005, 0.010, 0.020 and 0.030, HT at 1100 °C,

Table 1
Rietveld refinement data and crystallite size of $(Y_{0.995}Eu_{0.005})_4Al_2O_9$ powders heat-treated at 800 °C, 900 °C, 1000 °C, and 1100 °C.

Parameters	ICSD #63650 [31]	H.T. = 800 °C	H.T. = 900 °C	H.T. = 1000 °C	H.T. = 1100 °C
a **(Å)**	7.378	7.376 (7)	7.376(3)	7.379(2)	7.380(1)
b **(Å)**	10.474	10.460 (1)	10.458(4)	10.463(2)	10.465(1)
c **(Å)**	11.125	11.120 (1)	11.108(4)	11.109(3)	11.111(1)
β **(°)**	108.540	108.610 (5)	108.601(3)	108.601(2)	108.601(1)
V **(Å^3)**	815.1	813.0 (1)	812.1(6)	813.0(3)	813.3(2)
G_{of}	–	1.18	1.20	1.22	1.39
R_{wp} **(%)**	–	6.26	6.23	6.34	5.56
Crystallite size (nm)	–	34	48	86	120

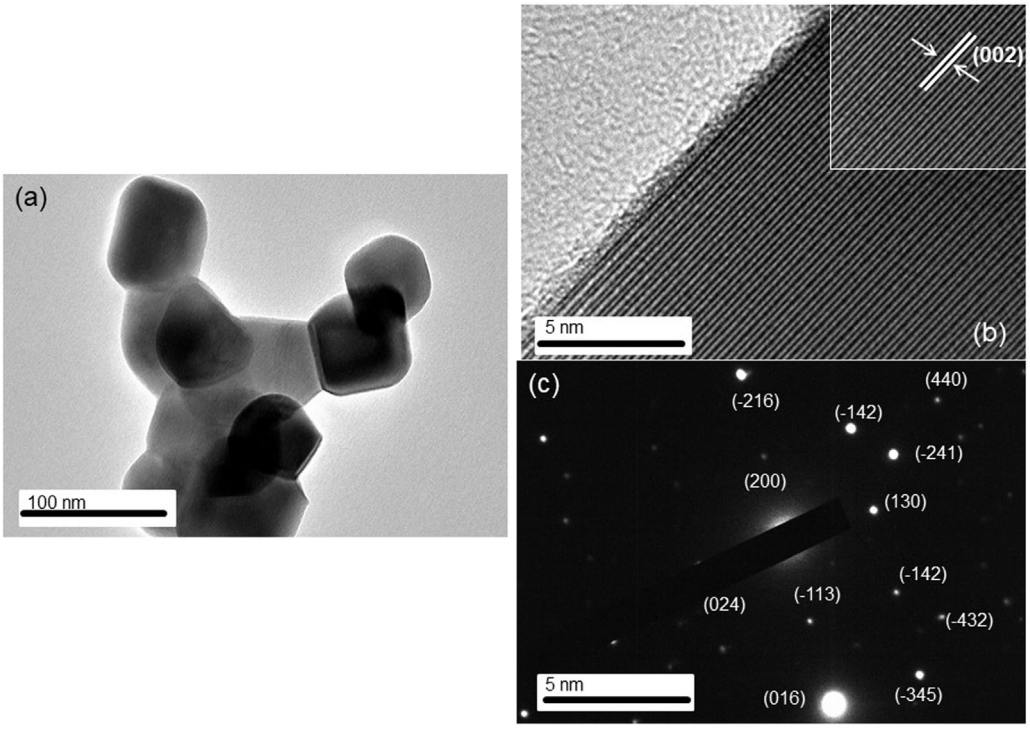

Fig. 2. (a) TEM, (b) HR-TEM, and (c) SAED images of $(Y_{0.995}Eu_{0.005})_4Al_2O_9$ powder heat-treated at 1100 °C.

monitoring the emission at 610 nm from Eu^{3+} $^5D_0 \rightarrow {}^7F_2$ transition. The narrow bands around 361, 380, 393, 413, 465, 530, and 583 nm are attributed to the 4*f*–4*f* transitions of the Eu^{3+} $4f^6$ configuration [20]. These peaks are assigned to the transitions $^7F_0 \rightarrow {}^5D_4$ (361 nm), $^7F_0 \rightarrow {}^5D_{2-6}$ (380 nm), $^7F_0 \rightarrow {}^5L_6$ (393 nm), $^7F_0 \rightarrow {}^5D_3$ (413 nm), $^7F_0 \rightarrow {}^5D_2$ (465 nm), $^7F_0 \rightarrow {}^5D_1$ (530 nm), and $^7F_0 \rightarrow {}^5D_0$ (583 nm). For concentrations the strongest peak is located at 393 nm. The main difference was observed for the band at 465 nm, the two peaks collapse and reduce their intensity in comparison to that at 393 nm for x = 0.30, indicating that the Eu^{3+} surroundings have been changed. Another feature is observed for $^7F_0 \rightarrow {}^5D_0$ transition, which is not only at 583 nm, but also others narrow and centered at 577 and 588 nm, probably mainly due to three different microenvironments for Eu^{3+} ions. It is reasonable suppose that the YAM lattices possess 3 different sites of Y^{3+} which could accommodate Eu^{3+}, in good agreement with the work developed by Kaczkan et al. [3]. Only 393 nm excitation was used to collect emission spectra due to its dominant intensity in all samples.

Fig. 4b illustrates the emission PL spectra of $(Y_{1-x}Eu_x)_4Al_2O_9$ powders with x = 0.001, 0.005, 0.010, 0.020 and 0.030, HT at 1100 °C. Under excitation at 393 nm, corresponding to Eu^{3+} $^7F_0 \rightarrow {}^5L_6$ transition (4*f* - 4*f* transitions), typical Eu^{3+} emissions from the $^5D_0$ to $^7F_0$, $^7F_1$, $^7F_2$, $^7F_3$, and $^7F_4$ levels were measured between 570 nm and 720 nm.

The most intense peak transitions are located around 610 nm (red emission-R) and around 590 nm (orange emission-O), corresponding to the $^5D_0 \rightarrow {}^7F_2$ and $^5D_0 \rightarrow {}^7F_1$ transitions, respectively. The intensity relation between red and orange emissions (R/O or $(^5D_0 \rightarrow {}^7F_2)/(^5D_0 \rightarrow {}^7F_1)$ relation) is 1.69 for x = 0.010, indicating that the europium ions are distributed in relatively low symmetry sites of the host, and the presence of the emission band at 579 nm assigned to the $^5D_0 \rightarrow {}^7F_0$ attests a chemical environment without an inversion center. In addition, splitting was observed in the $^5D_0 \rightarrow {}^7F_0$ transition (from 574 to 582 nm; see inset in Fig. 4b) and an inhomogeneous broadening, which suggests a distribution of Eu^{3+} ions in more than three symmetry sites into the host. Furthermore, the emission spectra profile considering all $^5D_0 \rightarrow {}^7F_J$ (J = 0, 1, 2, 3, 4) transitions is broadened, which can be attributed to the effect of the distribution of different microenvironments around the Eu^{3+} ion, that is, distinct symmetry sites occupied by the Eu^{3+} ions in the host, producing inhomogeneous broadening due to the superposition of Stark emission levels. As the YAM matrix possesses a monoclinic structure having a $P2_1/c$ space group, composed of AlO_4 tetrahedra sites, and two YO_6 and two YO_7 polyhedra sites, this can lead us to think that mostly Eu^{3+} prefer substitutes Y^{3+} in YO_6 and YO_7 polyhedra sites of the YAM structure.

The $^5D_0$ level emission PL decay curve of Eu^{3+} ions under excitation at 393 nm and a non-single exponential decay is observed (see Fig. 5). To calculate the average lifetime (τ_{ave}) value of the $^5D_0$ excited state, we integrated the decay curve using the equation: [20]

$$\tau_{ave} = \int_{t_0}^{t_f} \frac{I(t)}{I(t_0)} dt \quad (5)$$

All obtained values are listed in the Table 2, changing from 4.41 ms to 3.12 ms for x = 0.001 and x = 0.030, respectively.

However, the emission PL decay curves were fitted with some exponential curves, and good results were reached by considering two exponential curves, with lifetime of τ_1 = 5.254 ms and τ_2 = 1.491 ms, and pre-exponential factors A_1 = 0.759 and A_2 = 0.241, respectively, for x = 0.001; and τ_1 = 3.473 ms and τ_2 = 1.180 ms, and pre-exponential factors A_1 = 0.829 and A_2 = 0.171, respectively, for x = 0.030. All lifetime and pre-exponential values are listed in the Table 2. These results suggest that at least two main sites contributed to the transition. The first one, corresponding to the longer lifetime, is possibly due to Eu^{3+} ions replacing YO_7 sites of the YAM monoclinic structure, which is consistent with presence of Eu^{3+} in relatively low symmetry site (as long as 3.473 ms), probably a distorted octahedral site and low phonon energy. Nonetheless, the fast component can be assigned to Eu^{3+} in YO_6 sites with a higher phonon energy of the YAM monoclinic structure. The faster one has a lower pre-exponential factor than that calculated for the other component, demonstrating that higher amounts of Eu^{3+} are isolated and well distributed into the YAM crystalline structure.

All lifetime values of $^5D_0$ level determined in this work are higher than those found in the literature, as we can see in the comparison in Table 2. Note that Kaczkan et al. [19] obtained three different values

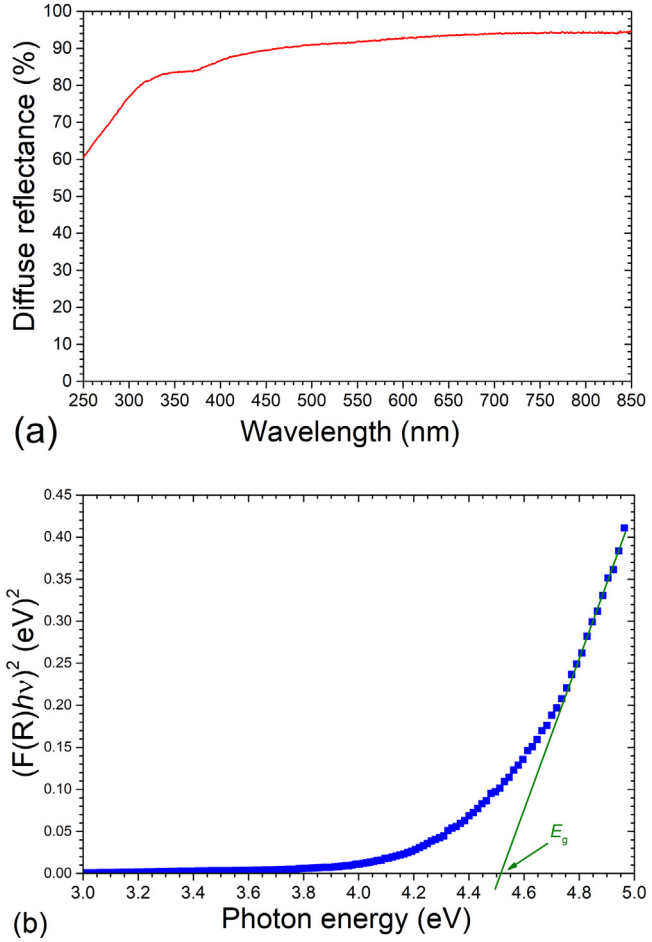

Fig. 3. (a) Diffuse reflectance spectrum as a function of wavelength and (b) $(F(R))h\nu)^2$ as a function of photon energy to band gap determination of $(Y_{0.995}Eu_{0.005})_4Al_2O_9$ powders heat-treated at 1100 °C.

(one for each site) between 2.22 and 3.57 ms for x = 0.006 doping. Increasing the Eu^{3+} concentration (from x = 0.045 to x = 0.200) [6,13,16], the lifetime reduced from 2.60 ms to 1.03 ms, as expected due to strong ion–ion interaction. In our study, we observed higher values because a lower Eu^{3+} concentration was used and, most likely, due to lower hydroxyl groups and structural defects in our materials than for those in the literature.

The Judd–Ofelt theory allow to predict oscillator strengths in absorption and luminescence, luminescence branching ratios, excited-state radiative lifetimes, energy-transfer probabilities, and estimates of quantum efficiencies by using only three parameters, Ω_λ (λ = 2, 4, 6) [38]. The traditional methodology require the absorption spectrum of each studied sample, and absorption coefficient should be determined, being easy for bulk glasses and monocrystals. However, for powdered samples, we cannot measure absorption coefficient and make traditional Judd-Ofelt calculations. Nevertheless, using the procedure described below, Werts and collaborators [39] and Carlos and colleagues [40] calculated the spontaneous emission probability (A), radiative lifetime (τ_{Rad}), quantum efficiency for $^5D_0 \rightarrow {}^7F_2$ emission, and Ω_2 and Ω_4 parameters and already that the procedure had been used for other Eu^{3+} doped materials [20,34].

The pure magnetic-dipole character of the $^5D_0 \rightarrow {}^7F_1$ transition enables the determination of the intensity parameters from the emission spectrum. As this transition does not depend on the local ligand field experienced by Eu^{3+} ions, it can be used as a reference for the entire spectrum 20,34,39,40]. The A_{01} spontaneous decay rate for the $^5D_0 \rightarrow {}^7F_1$ transition is $A_{01} = A'_{01} \cdot n^3$, where $A'_{01} = 14.65\ s^{-1}$ in vacuum and n

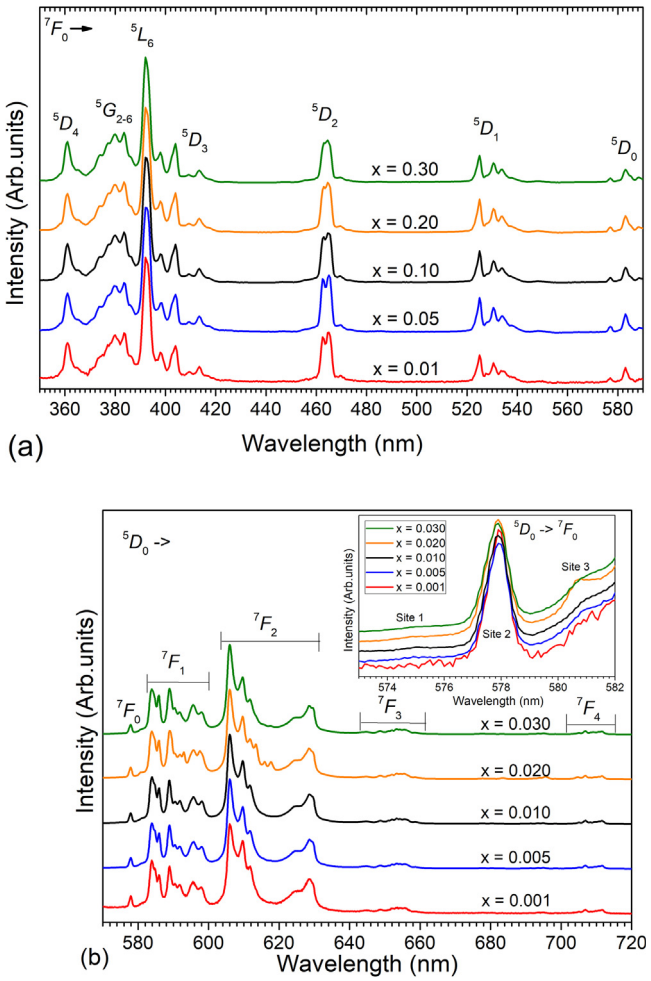

Fig. 4. (a) Excitation monitoring emission at 610 nm and (b) emission PL spectra under excitation at 393 nm for the $(Y_{1-x}Eu_x)_4Al_2O_9$ compositions with x ranging from 0.001 to 0.030, heat-treated at 1100 °C.

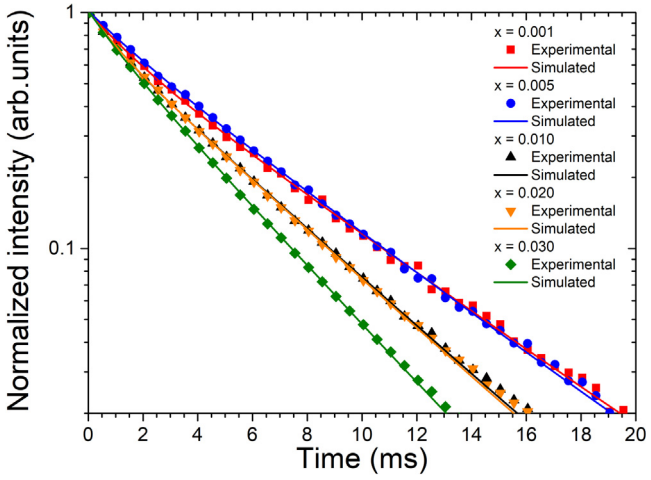

Fig. 5. PL decay curves for the $(Y_{1-x}Eu_x)_4Al_2O_9$ composition with x ranging from 0.001 and 0.030 heat treated at 1100 °C excited at 393 nm.

is the refractive index of the host material. Then, the intensity of the $^5D_0 \rightarrow {}^7F_{0-6}$ transitions in terms of the area of the emission curves (S_{0J}) is:

$$S_{0J} = hc\bar{u}A_{0J}N(5_{D0}) \quad (6)$$

where $N(^5D_0)$ is the $^5D_0$ level population that emits. The total radiative

Table 2
R/O relation, decay lifetimes and the amplitudes at zero time of $^5D_0 \rightarrow {}^7F_2$ transition of Eu^{3+} ions in monoclinic YAM powders with monoclinic structure, obtained at 1100 °C, and a comparison with lifetime values from the literature.

x value	*R/O relation*	τ_{ave} (± 0.05 ms)	τ_1 (ms)	τ_2 (ms)	A_1	A_2
0.001	1.65	4.41	5.254	1.491	0.759	0.241
0.005	1.68	4.55	5.089	1.886	0.813	0.187
0.010	1.69	3.64	4.160	1.018	0.812	0.188
0.020	1.62	3.62	4.123	1.030	0.820	0.180
0.030	1.57	3.12	3.473	1.180	0.829	0.171
0.006 (from [19] for site 1)	–	3.57	–	–	–	–
0.006 (from [19] for site 2)	–	2.22	–	–	–	–
0.006 (from [19] for site 3)	–	2.93	–	–	–	–
0.045 (from [6])	–	2.60	–	–	–	–
0.060 (from [13])	–	1.81	–	–	–	–
0.200 (from [16])	–	1.03	–	–	–	–

decay rate can be written as:

$$A_T = \sum_{J=0}^{6} A_{0J} = \frac{A_{01} h c \upsilon_{01}}{S_{01}} \sum_{J=0}^{6} \frac{S_{0J}}{h c \upsilon_{0J}} \quad (7)$$

The branching ratio for the $^5D_0 \rightarrow {}^7F_{5,6}$ transitions must be neglected owing to its low relative intensity, and the radiative contribution can be calculated using only the $^5D_0 \rightarrow {}^7F_{0-4}$ transitions [20,34,40].

The emission quantum efficiency (qe) is defined by the experimental and radiative lifetime ratio [20,34,40]:

$$qe = \frac{\tau_{ave}}{\tau_{rad}} \quad (8)$$

The site symmetry and luminescence behavior of Eu^{3+} ions in the matrix was carried out by calculating the J-O parameters Ω_λ ($\lambda = 2, 4$). In the J-O theory, the intensity parameters Ω_λ are given as [20,34,39,40]:

$$\Omega_\lambda = \frac{3}{64} \frac{h}{\pi^4 e^2 \upsilon^3} \frac{9}{n(n^2+2)^2} \frac{1}{|\langle 5D0 \| U^{(\lambda)} \| 7FJ \rangle|^2} A_{0J} \quad (9)$$

The values for the reduced matrix elements are 0.0032 for $\lambda = J = 2$ and 0.0023 for $\lambda = J = 4$. Table 3 lists the determined values for A_{01}, A_{02}, A_{04}, A_T, τ_{rad}, qe(%), Ω_2 and Ω_4. For the calculation, we considered the refractive index (n) of 1.70 from Lancok et al. [41]. The emission quantum efficiency was calculated using the τ_{ave} value, as listed in Table 3.

The photon density changes in an optically dense medium [42], and Eu^{3+} - Eu^{3+} interaction effects leading to lifetime reduction and PL quenching. Therefore, the $^5D_0$ radiative average lifetime of Eu^{3+} decreases or the radiative transition rates increases, as seen in Table 3.

In this way, the quantum efficiency (qe) of the $^5D_0 \rightarrow {}^7F_2$ transition is higher for samples with low Eu^{3+} concentration (Table 3). When the τ_{ave} is used, the estimated qe value is about 93% for x = 0.005; clearly, the presence of a non-radiative process was considered here. However, Taking into account the two experimental lifetimes by fitting the decay curve to a bi-exponential function, qe values obtained for τ_1 and τ_2 were 87% and 32%, respectively, for x = 0.005%, and 69% and 17%, respectively, for x = 0.020. Likely, both lifetimes are due to the Eu^{3+} replacing Y^{3+} of YO_7 and YO_6 polyhedra, respectively. These results indicate that a high portion of Eu^{3+} ions is located in a well-protected site with low phonon energy.

The polarization and asymmetry behavior of rare-earth ligands are determined by the Ω_2 parameter, whereas Ω_4 depends on long-range effects [43]. The higher Ω_2 value for Eu^{3+} in x = 0.010 indicates a highly asymmetric nature, corroborated by the higher R/O ratio of 1.69, which is probably related to good distribution of ions in different sites. The low Ω_4 value implies that $^5D_0 \rightarrow {}^7F_2$ transition efficiency increases, and this transition accounts for the majority of Eu^{3+} emission, resulting in these materials with high red emission ($^5D_0 \rightarrow {}^7F_2$ transition), especially for x = 0.010.

Analyzing in more detail, the $^5D_0 \rightarrow {}^7F_0$ transition that connects two non-degenerated levels and its band quantity reflects the quantity of occupied sites by Eu^{3+} ions [3], as we can observe in the Fig. 4b inset, with only one band centered at 578 nm for x = 0.001, as already reported in literature [6,8,9]. However, for samples with x ≥ 0.005, we observed three bands, centered at 575 nm, at 578 nm and at 580.5 nm, which can be attributed to three different occupation sites for Eu^{3+} ions, as similarly found by Kaczkan et al. [3]. For site 3 (emission centered at 580.3 nm), its intensity increased from x = 0.001 to x = 0.020 but decreased for x = 0.030, corresponding to quenching concentration. In the sample with x = 0.030, this occurred because there is a strong interaction between neighbour Eu^{3+} ions, leading to emission PL and lifetime reductions.

For the $^5D_0 \rightarrow {}^7F_1$ transition, it is noted seven sub-bands are due to the Stark effect. This transition exhibits a magnetic dipole (MD) feature and is allowed by selection rules independent of local symmetry. According to the crystalline field theory, the maximum values of each level are $2J + 1$, that is, we would have only three sub-bands per site of YAM structure or, if Eu^{3+} occupied three different sites, it would lead us to see nine sub-bands, but two of them can be superposed to others.

The $^5D_0 \rightarrow {}^7F_2$ transition is a forced electric dipole (ED) type. This is a hypersensitive transition, and its intensity can vary depending on the local environment of Eu^{3+} ions. If this hypersensitive transition presents higher emission intensity than other transitions, then the Eu^{3+} ions are located in the crystallographic site without a symmetry center. According to the crystalline field theory, this transition should have five broad sub-bands, as observed for x = 0.001, 0.005, 0.010 and 0.030; however, the sample with x = 0.020 presented eight sub-bands. This is an indication that Eu^{3+} ions occupy different sites in the sample, with x = 0.020 being the best composition with well-dispersed ions. Note

Table 3
Judd-Ofelt parameters, quantum efficiency, and intensity parameters for $^5D_0$ state under excitation at 394 nm.

x value	A_{01} (s^{-1})	A_{02} (s^{-1})	A_{04} (s^{-1})	A_T (s^{-1})	τ_{rad} (ms)	τ_{ave} (ms)	qe (%)	Ω_2 (10^{-20} cm^2)	Ω_4 (10^{-20} cm^2)
0.001	74.418	122.053	5.132	201.603	4.96	4.41	89	2.642	0.170
0.005	74.431	126.437	4.422	205.290	4.87	4.55	93	2.730	0.148
0.010	74.457	126.682	4.248	205.387	4.87	3.64	75	2.735	0.142
0.020	74.339	121.007	4.929	200.275	4.99	3.62	73	2.622	0.161
0.030	74.392	117.580	4.576	196.548	5.09	3.12	61	2.538	0.153

that the emission intensity, by integrating from 570 nm to 720 nm, increase continuously from x = 0.001 to x = 0.020 and decreased for x = 0.030. All these features show that concentration quenching is between x = 0.020 and x = 0.030, as confirmed by the reduction of Ω_2 values (Table 3) that present a maximum for x = 0.010.

M.P. Hehlen et al. [38] mentioned that clear correlations are difficult to establish because the coordinating environment has only a small influence on the well-shielded 4*f* electrons, and the intensities of specific 4*f*–4*f* transitions generally varies by a factor of two at most. A variety of models have been suggested over the years regarding the physical origin of this correlation, and trends in Ω_λ intensity parameters have been studied extensively for rare-earth ions doped glasses, for which a large compositional space is accessible [38].

In a general way, Ω_2 value indicates the symmetry site for Eu^{3+} ions, while the Ω_4 parameter indicates a change in the covalence degree, or Eu^{3+} ions in YAM structure are placed in relatively low symmetry sites and low covalence degree between Eu^{3+} and O^{2-} ions. Sample with x = 0.10 probably possess mainly Eu^{3+} ions occupying higher symmetry sites ($\Omega_2 = 2.735 \times 10^{-20}$ cm^2) and having lower covalence degree ($\Omega_4 = 0.142 \times 10^{-20}$ cm^2), when compared to other doping levels. Comparing our results from x = 0.10 sample (monoclinic Eu:YAM), the Ω_2 is higher and Ω_4 is lower than those determined for cubic Eu:YAG ($\Omega_2 = 0.66 \times 10^{-20}$ cm^2) and ($\Omega_4 = 1.35 \times 10^{-20}$ cm^2) by E. V. Vilejshikova at al. [44], it reveal multiplicity of YAM sites / different microenvironments due to its monoclinic crystalline structure. Unfortunately, there are not in the literature Ω_2 and Ω_4 values for Eu3+ doped YAM phase and we could not compare it.

4. Conclusions

$Y_4Al_2O_9$ (YAM) polycrystals doped with Eu^{3+} ions were successfully obtained using a modified polymeric precursors method with D-sorbitol as polymerizing agent at a temperature of 800 °C, which is 200 °C lower than found in the literature. Eu^{3+} doped YAM monoclinic structure was obtained from 800 °C to 1100 °C, with crystallite size of 34 nm for powders HT at 800 °C and 120 nm for those HT at 1100 °C. In fact, the crystallite size increased by increasing the HT temperature. All cell parameters calculated by Rietveld refinement are in good agreement with those in the literature, and the inclusion of Eu^{3+} did not significantly change the structure of the YAM phase. HRTEM results of powders HT at 1100 °C showed grains of ~ 80 nm diameter and a large agglomerate due to a coalescence effect, in the same magnitude order of that determined by Scherrer's equation using X-ray diffraction patterns. The materials are non-conducting and the $(Y_{0.995}Eu_{0.005})_4Al_2O_9$ sample has an optical bandgap 4.52 eV, in good agreement with the literature. All doped samples possess visible photoluminescence emission between 570 nm and 720 nm, under resonant excitation of Eu^{3+} at 393 nm, having emissions from the $^5D_0$ level to $^7F_0$, $^7F_1$, $^7F_2$, $^7F_3$ and $^7F_4$ levels, with highest emission due to $^5D_0 \rightarrow {}^7F_2$ transition, between 602 and 632 nm. The experimental evidence of the existence of three occupation sites by Eu^{3+} ions was observed on the emission spectra analysis, calculated J-O parameters and determined lifetime of $^5D_0$ level. The concentration quenching effect was determined to be between x = 0.020 and x = 0.030 through the PL emission intensities and confirmed by the J-O intensity parameters. Our results suggest that the best sample is certainly that one with x = 0.020 $(Y_{0.980}Eu_{0.020})_4Al_2O_9$, which seems to be useful as red phosphors for display and LED, under excitation at ultraviolet light.

Acknowledgements

This research project is supported by the CAPES, CNPq, FAPEG, and FINEP Brazilian agencies. The authors thank Prof. Dr. Sidney J.L. Ribeiro from IQ-UNESP for providing the equipment to collect lifetime decay curves (HORIBA Jobin Yvon Fluorolog FL-3–222 spectrofluorometer), and the UFG LabMic (*Laboratório de Microscopia de Alta Resolução*) for providing transmission electron microscopy technique (TEM, HR-TEM, and SAED images). Lauro J.Q. Maia is the recipient of a scholarship (*Bolsa de estudos)* from CAPES/*Estágio Sênior/ Processo* no. 88881.121134/2016-01.

References

[1] B. Cockayne, J. Less-Common Met. 114 (1985) 199.
[2] J.F. Carvalho, F.S. De Vicente, N. Marcellin, P. Odier, A.C. Hernandes, A. Ibanez, J. Therm. Anal. Calorim. 96 (2009) 891.
[3] M. Kaczkan, S. Turczynski, D.A. Pawlak, M. Wencka, M. Malinowski, Opt. Mater. 58 (2016) 412.
[4] P. Upadhyay, D. Verma, A. Bourase, D.S. Prasad, V. Dubey, R. Tiwari, R.K. Tamrakar, Y. Parganiha, J. Kaur, Int. J. Lumin. Appl. 5 (2015) 239.
[5] J. Ma, Z. Yu, D. Zhang, J. Fan, W. Fu, J. Chen, S. Cai, B. Wang, J. Am. Ceram. Soc. 98 (2015) 370.
[6] H.C. Jung, J.Y. Park, G.S.R. Raju, J.H. Jeong, B.K. Moon, J.H. Kim, H.Y. Choi, Curr. Appl. Phys. 9 (2009) S217.
[7] D.Y. Wang, Y.H. Wang, J. Alloy. Compd. 425 (2006) L5.
[8] S. Liu, Q. Su, J. Alloy. Compd. 255 (1997) 102.
[9] P.J. Yadav, N.D. Meshram, C.P. Joshi, S.V. Moharil, Int. J. Chem. Phys. Sci. 2 (2013) 12.
[10] V. Dubey, J. Kaur, Y. Parganiha, N.S. Suryanarayana, K.V.R. Murthy, Appl. Radiat. Isot. 110 (2016) 16.
[11] C.D. Brandle, H. Steinfink, Inorg. Chem. 8 (1969) 1320.
[12] Y. Xi-Ming, X. Yong-Sheng, Y. Jiang-Bo, W. Yong-Qian, W. Hong-Mei, J. Wuhan. Univ. Technol. 18 (2003) 41.
[13] E.J. Nassar, L.R. Avila, P.F.S. Pereira, O.J. Lima, L.A. Rocha, C. Mello, K.J. Ciuffi, Quím. Nova 28 (2005) 238.
[14] E.J. Nassar, L.R. Avila, P.F.S. Pereira, C. Mello, O.J. Lima, K.J. Ciuffi, L.A. Carlos, J. Lumin. 111 (2005) 159.
[15] G. Xia, S. Zhou, J. Zhang, S. Wang, H. Wang, J. Xu, J. Non-Cryst. Solids 351 (2005) 2979.
[16] R. Yadav, A.F. Khan, A. Yadav, H. Chander, D. Haranath, B.K. Gupta, V. Shanker, S. Chawla, Opt. Express 17 (2009) 22023.
[17] D.F.D. Santos, M.E.G. Valerio, Sci. Plena 7 (2011) 074802.
[18] V. Dubey, S. Agrawal, J. Kaur, Appl. Radiat. Isot. 110 (2016) 16.
[19] M. Kaczkan, Opt. Mater. 59 (2016) 60.
[20] M.P.S. Almeida, L.M. Nunes, R.R. Gonçalves, S.J.L. Ribeiro, L.J.Q. Maia, Opt. Mater. 62 (2016) 438.
[21] A.F. Silva, F. Elan, E.L. Falcão-Filho, L.J.Q. Maia, C.B. de Araújo, J. Mater. Chem. C 5 (2017) 1240.
[22] L.J.Q. Maia, F.M. Faria Filho, V. Jerez, A.L. Moura, C.B. de Araújo, J. Mater. Chem. C 3 (2015) 11689.
[23] A.L. Moura, V. Jerez, L.J.Q. Maia, A.S.L. Gomes, C.B. de Araújo, Sci. Rep. 5 (2015) 13816.
[24] L. Marciniak, A. Bednarkiewicz, Sens. Actuators B-Chem. 243 (2017) 388.
[25] R. Matos, D. Liang, J. Almeida, B.D. Tibúrcio, C.R. Vistas, Opt. Commun. 420 (2018) 6.
[26] E. Kaewnum, N. Wantana, J. Kaewkhao, Mater. Today Commun. 5 (2018) 13954.
[27] J.F. Carvalho, F.S. De Vicente, S. Pairis, P. Odier, A.C. Hernandes, A. Ibanez, J. Eur. Ceram. Soc. 29 (2009) 2511.
[28] M. Gajc, H.B. Surma, A. Klos, K. Sadecka, K. Orlinski, A.E. Nikolaenko, K. Zdunek, D.A. Pawlak, Adv. Funct. Mater. 23 (2013) 3443.
[29] Y.H. Zhou, J. Lin, S.B. Wang, H.J. Zhang, Opt. Mater. 20 (2002) 13.
[30] Y. Shi, M. Zhong, Z. Zhang, D. Wang, Ceram. Int. 43 (2017) 5979.
[31] M.S. Lehmann, A.N. Christensen, H. Fjellvag, J. Appl. Crystallogr. 20 (1987) 123.
[32] H.P. Klug, L.E. Alexander, X-Ray Diffraction Procedures, Wiley, New York, 1954.
[33] L.J.Q. Maia, M.I.B. Bernardi, A.R. Zanatta, A.C. Hernandes, V.R. Mastelaro, Mater. Sci. Eng. B 107 (2004) 33.
[34] L.J.Q. Maia, F.M. Faria Filho, R.R. Gonçalves, S.J.L. Ribeiro, Opt. Mater. 75 (2018) 297.
[35] B. Hapke, Theory of Reflectance and Emittance Spectroscopy, Cambridge University Press, 2012.
[36] W.Y. Ching, Y.N. Xu, Phys. Rev. B 59 (1999) 12815.
[37] E. Talik, A. Guzik, P. Zajdel, L. Lipinska, M. Baran, M. Szubka, Mater. Res. Bull. 83 (2016) 56.
[38] M.P. Hehlen, M.G. Brik, K.W. Kramer, J. Lumin. 136 (2013) 221.
[39] M.H.V. Werts, R.T.F. Jukes, J.W. Verhoeven, Phys. Chem. Chem. Phys. 4 (2002) 1542.
[40] L.D. Carlos, R.A.S. Ferreira, V. Zea Bermudez, S.J.L. Ribeiro, Adv. Mater. 21 (2009) 509.
[41] J. Lancok, M. Jelinek, F. Flory, Proc. SPIE 3571, in: Tenth International School on Quantum Electronics: Laser Physics and Applications, 7 May 1999. ⟨http://dx.doi.org/10.1117/12.347653⟩.
[42] G. Pan, H. Song, Q. Dai, R. Qin, X. Bai, B. Dong, L. Fan, F. Wang, J. Appl. Phys. 104 (2008) 084910.
[43] S. Som, A.K. Kunti, V. Kumar, V. Kumar, S. Dutta, M. Chowdhury, S.K. Sharma, J.J. Terblans, H.C. Swart, J. Appl. Phys. 115 (2014) 1931011.
[44] E.V. Vilejshikova, A.A. Khort, K.B. Podbolotov, P.A. Loiko, V.I. Shimanski, S.N. Shashkov, K.V. Yumashev, J. Appl. Spectrosc. 84 (5) (2017) 866.